The spinning Astrid-2 satellite used for modeling the Earth's main magnetic field

Merayo, José M.G.; Jørgensen, P.S.; Risbo, T.; Brauer, Peter; Primdahl, Fritz; Cain, J.

Published in:
I E E E Transactions on Geoscience and Remote Sensing

Link to article, DOI:
10.1109/TGRS.2002.1006371

Publication date:
2002

Document Version
Publisher's PDF, also known as Version of record

The Spinning Astrid-2 Satellite Used for Modeling the Earth's Main Magnetic Field

Jose M. G. Merayo, Peter Brauer, Fritz Primdahl, Peter S. Joergensen, Torben Risbo, and Joe Cain

***Abstract*—The Swedish micro-satellite Astrid-2 was successfully launched into a near polar orbit in December 1998. Despite the fact that the primary science mission was auroral research, the magnetic instrument was designed to accomplish high-resolution and high-precision vector field magnetic measurements, and therefore mapping of the Earth's magnetic field was possible. The spacecraft spins about a highly stable axis in space. This fact and the globally distributed data make the magnetic measurements well suited for the estimate of a magnetic field model at the spacecraft altitude (about 1000 km). This paper describes the initial analysis of the Astrid-2 magnetic data. As a result of the study of a single day (February 7, 1999), magnetically fairly quiet, it was possible to in-flight adjust the calibration of the magnetometer and find a magnetic field model fitting the scalar component of the measurements to better than 5 nT_{rms} for latitudes Equatorward of 50°. Several methods for field modeling are discussed in this paper under the assumption that the direction of the spin axis in inertial space is nearly constant, and this assumption is corroborated by the observations. The approximate inertial orientation of the magnetometer could then be determined simultaneously with the instrument intrinsic calibration and the estimate of main field model coefficients. Hence, apart from the scientific use of the magnetic data, the attitude of the spacecraft may be estimated with high precision.**

***Index Terms*—Amorphous magnetic materials, calibration, data models, data processing, geomagnetism, geophysical inverse problems, magnetic fields, magnetic field measurement, magnetometers, measurement, modeling, satellites.**

NOMENCLATURE

ACS	Attitude control system.
ADC	Analog to digital converter.
ATV	Danish Academy of Technical Science.
CDC	Compact detector compensation.
CSC	Compact spherical coil.
DAC	Digital to analog converter.
DSP	Digital signal processor.
DTU	Technical University of Denmark.
DVD	Digital video device.
FTP	File transfer protocol.
IGRF	International geomagnetic reference field.
IMF	Interplanetary magnetic field.
KTH	Swedish Royal Institute of Technology.
MACOR	Machinable glass ceramic.
MAG	Magnetometer.
NASA	National Aeronautics and Space Administration.
NORAD	North American Aerospace Defense Command.
OVH	Overhauser magnetometer.
SIM	Star imager.
SSC	Swedish Space Corporation.
STVF	Danish Technical Scientific Research Board.
TLE	Two-line elements.
UT	Universal time.
WDC	World Data Center.

Manuscript received August 1, 2001; revised January 4, 2002. This work was supported in part by the Danish Technical Scientific Research Board (STVF) under Grants 9 502 705 and 26 00 0015, the Danish Academy of Technical Science (ATV) and Terma Elektronik AS, the "Magnetsrode" test facility of the Institute of Geophysics and Meteorology, the Technical University of Braunschweig (Germany), the Danish Meteorological Institute's Magnetic Observatory at Brorfelde (Denmark), the Swedish Geological Survey's Magnetic Observatory at Lovoe near Stockholm (Sweden), the Swedish Space Corporation, and the Swedish Royal Institute of Technology (KTH).

J. M. G. Merayo, P. Brauer, and P. S. Joergensen are with the Oersted·DTU, Technical University of Denmark, 2800 Lyngby, Denmark (e-mail: jmm@oersted.dtu.dk).

F. Primdahl is with the Oersted·DTU, Technical University of Denmark, Building 327, 2800 Lyngby, Denmark. He is also with the Danish Space Research Institute, 2100 Copenhagen Oe, Denmark.

T. Risbo is with the Geophysical Department, Copenhagen University, 2100 Copenhagen Oe, Denmark.

J. Cain is with Geophysical Fluid Dynamics Institute, Florida State University, Tallahassee, FL 32306-4360 USA.

Publisher Item Identifier S 0196-2892(02)04588-6.

I. INTRODUCTION

THE NASA MAGSAT satellite (1979–1980) was the first satellite to accurately measure the three components of the Earth's magnetic field with dense global coverage [1]. The importance of periodic measurements of the geomagnetic field has been recognized for many different purposes within solid Earth physics and other disciplines. However, since MAGSAT, no other mission carrying accurate vector magnetic instrumentation has flown until the Astrid-2 satellite. Shortly after Astrid-2, the Danish Oersted mission was launched (February 23, 1999), as a dedicated geomagnetic mission.

The Astrid-2 high-resolution magnetic instrumentation, combined with the possibility of determining an inertial reference system for the magnetometer based on the spin stabilized spacecraft, and the near polar orbit at about 1000 km providing good global data coverage, makes the Astrid-2 magnetic data set unique for geomagnetic research. It is also worth mentioning that the Astrid-2 satellite orbital plane drifted relative to the Sun and swept all local times during the mission.

The paper first briefly describes the Astrid-2 satellite, its science three-axis fluxgate magnetometer, and some aspects of the magnetic calibration. Then, the processing of the flight data is introduced aiming at the in-flight calibration and the scalar magnetic field modeling. Finally, the properties of the magnetic vector data are analyzed and presented with some examples of the de-spun data, and the high-precision attitude recovery possibilities based on the magnetometer measurements and the vehicle dynamics are discussed.

The primary purpose of this paper is to demonstrate the feasibility of getting mapping quality vector magnetic field data from a small spinning satellite. The main field model presented below is for this purpose only and is not meant to compete with the IGRF. A secondary aim is to demonstrate the stability of the satellite spin axis, thereby supporting the possibility of modeling the absolute attitude of the magnetometer (and of the spacecraft) simultaneously with modeling the main field of the Earth.

II. The Astrid-2 Satellite

Astrid-2 is an advanced auroral microprobe with dual primary mission objectives: to do high-quality *in situ* measurements of the auroral physics processes, and to demonstrate the usefulness of micro-spacecraft as advanced research tools [2]. The mission has opened up entirely new possibilities for low-budget multipoint measurements in near-Earth space. These long-needed *in situ* measurements constitute the next major step forward in experimental space physics. Astrid-2 has platform dimensions of $45 \times 45 \times 30$ cm, a total mass of just below 30 kg, and carries scientific instruments for measuring local electric and magnetic fields, plasma density and density fluctuations, ions and electrons, as well as photometers for remote imaging of auroral emissions. Attitude determination was hoped to be provided by a high-precision star imager system (SIM), but for vehicle stability reasons a spin rate above the specified star camera operating range was chosen, and so the attitude determination had to rely on the less accurate (about 0.1°) pre-flight implemented back-up solution, based on the science magnetometer [3].

During the pre-flight satellite level magnetic calibrations (see below), the intercalibration between the star camera head and the magnetometer sensing unit was determined, resulting in a star based angular pointing accuracy of 6 arcsec between the magnetometer and the local magnetic field vector [4], [5].

Astrid-2 (Fig. 1) was launched on December 10, 1998 at UT 11:57:07 as a piggy-back payload on a Russian Kosmos-3M launcher from Plesetsk into an 82.9° inclination and almost circular orbit of 1015×978 km altitude with an orbital period of 105.1 min (this gives almost 14 orbits per day). Nodal regression gave complete coverage of all local time sectors every 3.5 months. Telemetry was lost on July 24, 1999 during a downlink connection and at present the cause is unexplained. Some 150 Mbytes' worth of scientific data was received each day at the two ground stations: Solna (Northern hemisphere, Sweden) and Sanae (Southern hemisphere, South African Antarctic base).

As mentioned above, the main objectives of the Astrid-2 mission are basically dedicated to the study of local phenomena related to electromagnetic waves in the plasma at the satellite altitude and their correlation with auroral arcs. The frequencies of interest lie in the range of dc to 400 Hz. The interchange of energy between the ionosphere and the magnetosphere can then be addressed by simultaneous observations from other spacecraft systems or from ground based instrumentation. Determination was made of external magnetic field sources and their dependence on local time, season, IMF conditions, and substorm activity. Model predictions of the electromagnetic weather were compared to actual observations, especially in the polar ionospheres. Statistical studies were made of the global distribution of E, B, and Birkeland currents. Of particular interest is to obtain representative $\mathbf{E}$- and $\mathbf{B}$-field distributions in the cusp region and in the Harang discontinuity region (produced by two electrojects with opposite directions near the mid-night sector) using simultaneous data.

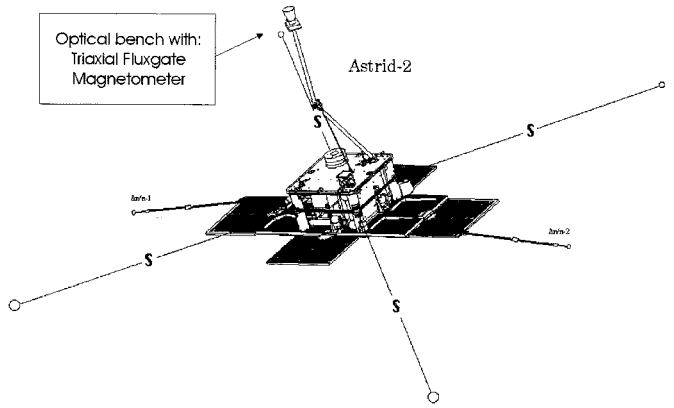

Fig. 1. Schematic picture of the Astrid-2 satellite in the flight configuration. All booms for the electrical probes, the 0.9-m axial boom for the MAG/SIM and the solar panels are shown deployed.

III. The Astrid-2 Magnetometer

The Astrid-2 magnetometer has a triaxial sensor unit consisting of three independent single-axis compensated fluxgates and is based on the CDC sensor design (Fig. 2). The magnetic material used in the sensor core is the amorphous metallic glass Vitrovac 6025 from Vacuumschmelze GmbH with virtually zero magnetostiction [6]. The support of the sensor is made of MACOR (Corning Incorporated) in order to have very good thermal properties [7].

The instrument is based on a digital signal processor (DSP) controlling all the timing processes of the magnetometer electronics [8]. The DSP generates all synchronizing signals for the excitation and the ADCs/DACs. The outputs of the detector coils of the individual fluxgate sensors are connected to signal conditioning preamplifiers and fed to 16-bit ADCs sampling several times faster than the excitation frequency. The digitized version of the signal is then correlated in the DSP with a matched reference signal. The maximum correlation value is proportional to the magnetic field sensed by the fluxgate transducer. The integrator and interpolator are also programmed in the DSPs, and the outcome of these computations are used to feed three DACs (also running fast in order to produce sufficient oversampling), and finally the feedback loops of the instrument are closed through voltage-to-current converters that feed the compensation currents to the detector coils. The fluxgate sensors are then used as null detection devices. The outputs of the DSP are selectable to 16, 256, and 2048 Hz with 20 bits of resolution. The detector coils' outputs are a fairly small out-of-balance signals superposed on the feedthrough and, therefore, can be digitized with fewer bits than the magnetometer output.

The range of the magnetometer is $\pm 62\,000$ nT in each component with a digitizing step of 0.12 nT. The sensor unit is

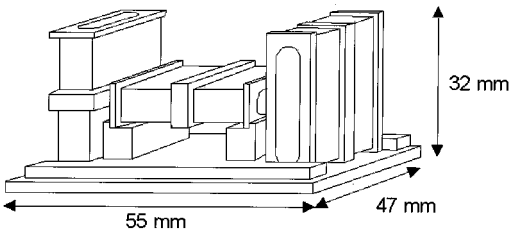

Fig. 2. The tri-axial assembly of the Astrid-2 CDC sensor unit. The sensor is further supplied with top and side plates. All parts are made of MACOR to have a mechanically rigid and thermally well-behaved sensor.

box-shaped measuring 45.4 × 53.4 × 33.0 mm and it weighs 150 g. The magnetometer electronics is contained on two 177 × 134 mm PCB's weighing in total 465 g and consuming 2 W. The 5 mm diameter sensor cable is a highly flexible and ultralow temperature type weighting 30 g/m. Table I summarizes all the magnetometer performance characteristics. The digitizing step limits the resolution of the magnetometer, which is greater than the instrument noise. But the low thermal coefficients ensure the high precision measurements.

Magnetic calibrations were performed at instrument level at the "Magnetsrode" test facility of the Institute of Geophysics and Meteorology, Technical University of Braunschweig, Germany, in the laboratory at DTU and at the Danish Meteorological Institute's Magnetic Observatory at Brorfelde, Denmark [7]. The final satellite-level magnetic calibration was performed at the Swedish Geological Survey's Magnetic Observatory at Lovoe near Stockholm, Sweden [4], [5]. The operating and near-flight configured satellite was exposed to the monitored Earth's field in about 60 different directions, and a scalar calibration was performed using the 48 first positions. Taking a local field gradient into account and compensating for the DAC nonlinearities, the overall standard deviation of the individual data points was 1.3 nT_{rms}. This includes all the perturbations from the satellite and the remaining nonlinearities in the sensor and the DACs. The instrument's band noise was below 50 pT_{rms} [8] at the 16-Hz output.

The Swedish Space Corporation (SSC) and all the instrument providers successfully complied with the magnetic cleanliness requests put up by the magnetometer team and the project. Tests at Lovoe confirmed the very low magnetic perturbations from the satellite by sequentially power-cycling the subsystems. The maximum perturbation came from the transmitter, causing 4 nT at the boom-deployed magnetometer sensor [9]. The data can then be cleaned for these well-defined events and identifiable perturbations.

The pre-flight calibration of the magnetometer provided the means to qualify and model the behavior of the instrument before launch. The magnetic field vector can be expressed as a linear function of the three raw 20-bit outputs of the magnetometer.

First, an orthogonal system is constructed by using the magnetic sensors as an intrinsic reference system frame [10]

$$\begin{aligned}\mathbf{i} &\equiv \mathbf{d}_1 \\ \mathbf{j} &\equiv \mathbf{k} \times \mathbf{d}_1 \\ \mathbf{k} &\equiv \frac{\mathbf{d}_1 \times \mathbf{d}_2}{|\mathbf{d}_1 \times \mathbf{d}_2|}.\end{aligned} \tag{1}$$

TABLE I
MAGNETOMETER PERFORMANCE CHARACTERISTICS

Range	± 62 000 nT
Resolution	0.12 nT (20 bits)
Sensor Noise	< 7 pT_{RMS} (0.05–10 Hz)
	(< 3 pT/√Hz at 1 Hz)
Sampling Rate	2 048 / 256 / 16 Hz
Power Consumption	2 W
a) Sensor Calibrated Performance (-45 °C to +15 °C)	
Offset stability	± 0.5 nT (long term)
Offsets tempcoeff.	0.02, 0.01, 0.46 nT/°C
Scale factors uncertainty	± 0.0025 % of full scale
Scale factors tempcoeff.	-13, -11, -11 ppm/°C
Axes' Intrinsic Orthogonality	± 15 arcsec (± 0.004 °)
Non-Orthogonality tempco.	0.17, 0.33, 0.53 arcsec/°C
b) Physical Properties	
Sensor dimensions	45.4 x 53.4 x 33.0 mm
Sensor weight	150 g
Electronics dimensions	2 PCB's 177 x 134 mm
Electronics weight	465 g
Cable weight	30 g/m

The Science Magnetometer of the Astrid-2 Satellite [7,8].

This indicates that the first orthogonal axis $\mathbf{i}$ is chosen along the direction of the first detector coil axis, $\mathbf{d}_1$. The third orthogonal axis $\mathbf{k}$ is perpendicular to the plane defined by the first and second coil axes, $\mathbf{d}_1$ and $\mathbf{d}_2$. The second orthogonal axis, $\mathbf{j}$, lies in the plane formed by $\mathbf{d}_1$ and $\mathbf{d}_2$, and it is perpendicular to $\mathbf{d}_1$. This completes the right-handed orthogonal system $\{\mathbf{i}, \mathbf{j}, \mathbf{k}\}$ associated with the nonorthogonal coil axes triad $\{\mathbf{d}_1, \mathbf{d}_2, \mathbf{d}_3\}$.

Second, the relation between the magnetic field components (M_1, M_2, M_3) and the magnetometer outputs can be approximated by a linear combination of the raw outputs in engineering units (digital bits) (EU_1, EU_2, EU_3), if the transverse effect is small [7]. The effect of the proximity of the three independent transducers forming the sensor is negligible, because this effect is absorbed into the calibration parameters [11]. Hence, the relationship for the Astrid-2 magnetometer is

$$\begin{bmatrix} M_1 \\ M_2 \\ M_3 \end{bmatrix} = \begin{bmatrix} a_{11} & 0 & 0 \\ a_{21} & a_{22} & 0 \\ a_{31} & a_{32} & a_{33} \end{bmatrix} \begin{bmatrix} EU_1 - O_1 \\ EU_2 - O_2 \\ EU_3 - O_3 \end{bmatrix}. \tag{2}$$

Here, $\mathbf{O}$ is the offset vector and a_{ij} are the components of the lower triangular calibration matrix.

IV. DATA SELECTION

There were two criteria for selecting the data: 1) the period had to be magnetically fairly quiet and 2) lack of ACS maneuvers. If the currents normally existing in the ionosphere and magnetosphere are enhanced as a result of perturbations driven by the Solar Wind, they cause changes in the magnetic field.

This cannot be described by a global model based on a scalar potential and on the nonexistence of such currents. The period chosen is the day of February 7, 1999. On this day the Kp index was less that 3+ for any of the three-hour intervals, and the sum for the whole day was 22−. The Ap index for this period was 13. These indexes were retrieved from [12]. The index measuring the state of the ring current Dst has also been retrieved from the World Data Center for Geomagnetism WDC-C2 at Kyoto [13], and it has a standard deviation value of 3 nT with a maximum value of −11 nT and a minimum of −23 nT.

The other constraint for selecting the data is the activity of the ACS. If the magnetic data is to be used for a vector field model, then the orientation of the satellite spin axis has to be stable in inertial space. This means that there should not be any large Attitude Control System (ACS) maneuvers. The Astrid-2 satellite is a spinner with the solar panels orientated approximately perpendicular to the Sun vector. When the angle between the spin axis and the Sun vector differs by more than a few degrees (caused by orbital plane drift), then the ACS takes action to correct this. The absence of ACS actions was actually the main reason for selecting February 7, 1999, despite the fact that the magnetic conditions were only moderately quiet.

The scalar value of the raw data for February 7, 1999, is depicted in Fig. 3. This has been computed using the pre-flight calibration without temperature correction. The thickening of the traces shows that the spin is not completely removed indicating that applying a simple pre-flight calibration set of parameters without temperature correction is not enough. The computed scalar magnetic field from the IGRF95 model extrapolated to the involved epoch is plotted on top of the curve but it is not visible due to the scaling. A magnified time series in shown on the left bottom side of the figure. There are some few outliers in the raw data indicated by the vertical lines stretching to the top or the bottom of the panel, and these have been eliminated before further analysis. The total number of Astrid-2 magnetic vectors for February 7, 1999, is 1 999 166 taken at both 16- and 256-Hz sampling rates. This dataset was subsampled by a factor of 8/128 if the sampling frequency was 16/256 Hz, respectively (taking every 8/128th vector) to 2 Hz giving 176 543 vectors. There were 82 outliers in the subsampled data amounting to a total of $<0.05\%$.

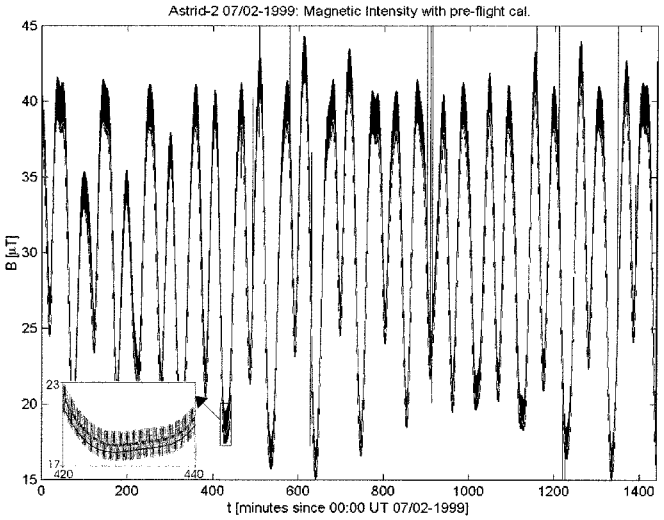

Fig. 3. Astrid-2 magnetic intensity for the day of 07/02-1999 computed from the magnetometer outputs using pre-flight calibration. The computed scalar magnetic field from the IGRF95 model extrapolated to the involved epoch is plotted on top of the curve (visible only in the magnified trace on the left bottom side).

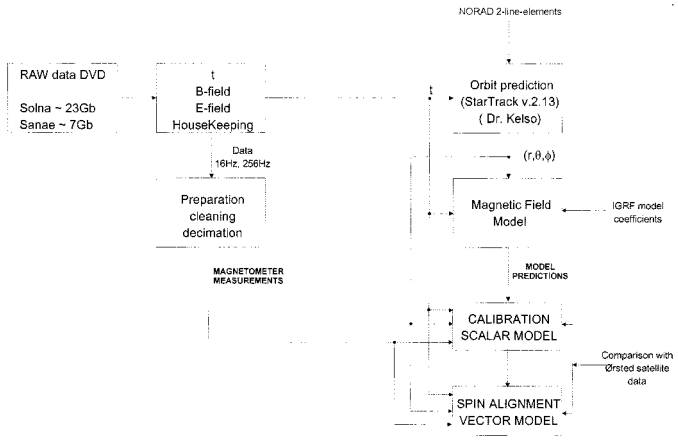

Fig. 4. Block diagram showing the steps for organizing the Astrid-2 data set for Magnetic Main Field investigation.

V. Data Preprocessing

Presently, a complete copy of the data from the Solna (Northern hemisphere) and Sanae (Southern hemisphere) ground stations exists at Oersted·DTU. This represents about 30 Gbyte of raw data from the downlink telemetry stored in DVD format. Subroutines for extracting the necessary information from the data have been developed and implemented. The block diagram in Fig. 4 represents schematically the process by which the data is used. This includes the magnetic scientific data (and $\mathbf{E}$-field probe data where needed), the time relative to the satellite internal counter and the housekeeping data of the magnetometer with the temperatures of the sensor and of the electronics. The readings from the Sun sensor are also extracted in order to have an initial estimate of the spin frequency and phase.

The $\mathbf{B}$-field data come at different rates. In normal mode, the magnetometer is sampling at 16 Hz. As the satellite crosses the auroral zones, the rate is switched to 256 Hz in order to observe the more variable auroral phenomena with a higher bandwidth. The 2048-Hz sampling mode is rarely used in space, because of limitations in the internal memory. The delay that occurs by switching between the 16-Hz and 256-Hz modes is corrected for when extracting the data from the raw data files.

Each of the magnetometer samples is associated with a time-stamp that is related to a specific initial time, which corresponds to the time when the Astrid-2 main computer was last reset. In order to determine accurately the internal time relative to the Universal Time (UT), the satellite computer records the value of the counter when there is a contact with the ground station. The counter frequency can be established with high precision during a downlink, since it is related to the satellite oscillator. A table relating this time to UT is available from the project and is used for converting the relative time provided by the internal counter. The time-table error is stated by the project to be

less than 0.1 s in the worst case. This corresponds to less than 700 m in position along the orbit and to less than 1.5 nT in the scalar field, which is comparable with the position accuracy discussed below. The switching between different sampling modes produces some fluctuations in the timestamps, which have to be compensated for. This is done by looking at the magnetic data that usually come equidistantly in time regardless of time stamp errors. If a correction was not possible, the magnetic vectors were disregarded. In order not to introduce any erroneous signals, the data has not been filtered when used in the geomagnetic modeling. Instead, the data is subsampled with a specific interval of 0.5 s between samples. This is still a tremendous amount of data and it is further subsampled by a factor of 100 (selecting every 100th sample, see Fig. 5), giving 1766 points that are used for further analysis.

The timestamp associated with each measurement was used to compute the position at which the observation was carried out, and, for this, information about the orbit is needed. The satellite did not carry any device for position determination and this was the reason to use orbit data from the North American Aerospace Defense Command (NORAD) who maintains general orbital element sets on all resident space objects. These element sets are periodically refined so as to maintain a reasonable prediction capability on all space objects. These element sets are "mean" values obtained by removing periodic variations in a particular way, and they are provided to users who then will have to reconstruct and re-introduce these periodic variations (by a prediction model) in exactly the same way as they were removed by NORAD. The software for this, StarTrack v2.1.3 is supplied by Dr. T. S. Kelso [14] and is capable of predicting the position of the satellite from the UT time and the orbital two-line-elements (TLEs) for the specific period, where the position is required.

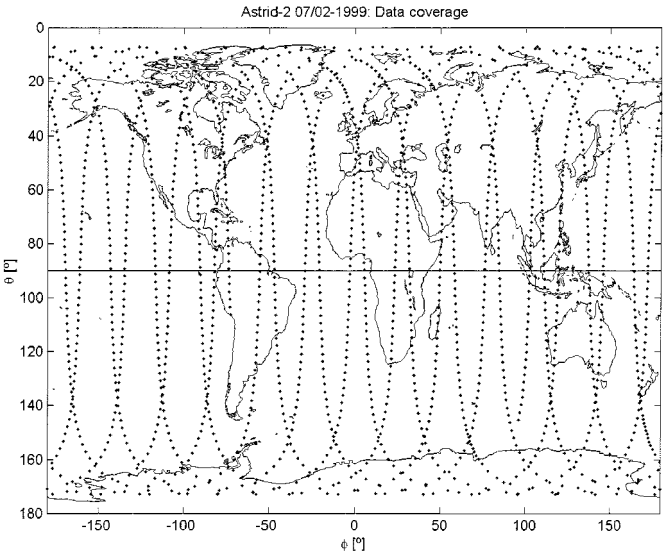

Fig. 5. Global coverage of the Astrid-2 data for 07/02-1999. The 256/16 Hz data is sub-sampled to 50 s without any post-filtering. The position is computed for each data point from the NORAD TLEs using the StarTrack prediction program.

VI. Magnetometer Calibration

The scalar calibration uses the field measured by a scalar magnetometer and the computed scalar field of the vector magnetometer that is parameterized by nine parameters for the case of a linear magnetometer like in (3). These parameters are: the three offsets, the three scale factors, and three nonorthogonal angles between individual axis. If the magnetometer is exposed to fields in all directions, it is possible to determine these nine parameters independently both on ground and in flight without knowing the external orientation of the magnetometer. This is used by MAGSAT and Oersted. However, Astrid-2 does not carry a scalar magnetometer and therefore, in-flight it has to used the input scalar field from the magnetic field model. During pre-flight calibration, the Astrid-2 satellite was set up at the Lovoe Magnetic Observatory of the Swedish Geological Survey on May 15–16, 1997. The vector magnetometer measured the Earth's magnetic field $\mathbf{B}$ while the satellite was oriented in 60 different directions with respect to the field by tilting and turning the whole satellite. At the same time the intensity of the $\mathbf{B}$-field was recorded with a scalar proton magnetometer. A comparison between the vector and scalar magnetometers was then made in a scalar calibration [4], [5], [10] and this gave the pre-flight calibration parameters used for transforming the raw data into components specified in terms of an intrinsic orthogonal sensor reference system based on the magnetometer sensor's physical magnetic axes (see Fig. 6).

As discussed above, the calibration was performed with the magnetometer on-board the flight configured and operating satellite. The pre-flight calibration parameters thus include the influences from the satellite and all instrument nonlinearities. The calibration coefficients are temperature dependent. Because of the tight schedule, only the Astrid-2 flight-spare magnetometer was thermally characterized at the "Magnetsrode" facility of the institute of Geophysics and Meteorology at the Technical University of Braunschweig, Germany. The sensitivities', the offsets', and the nonorthogonal angles' thermal coefficients for this magnetometer are -13, -11, -11 ppm/°C, 0.02, 0.01, 0.46 nT/°C and 0.17, 0.33, 0.53 arcsec/°C, respectively for the three axes [7]. These thermal coefficients are assumed to be the same for the flight sensor unit based on the identical construction and production.

The pre-flight calibration was checked in-flight by comparing the in-flight measurements with the predicted scalar magnetic field derived from the extrapolated IGRF95 model. The in-flight scalar calibration residuals based on 1766 data points and the scalar field computed from the IGRF95 extrapolated to the time of the data are shown in Fig. 7. The orbital temperature variations of the sensor only amounted to a few °C, and therefore, for this specific day, no thermal correction has been taken into account. After this in-flight adjustment of the pre-flight calibration, it was observed that the spin frequency was heavily attenuated in the scalar magnetic intensity residuals. The difference between in-flight and on-ground calibration parameters is due to the temperature at which they have taken place (below -30 °C and $+20$ °C, respectively). These are the result of the sensor and electronics thermal effects and are of the order of 50 ppm/°C. The standard deviation of the single points in Fig. 7 is about 18 $\mathrm{nT_{rms}}$ reflecting, among other things, the differences

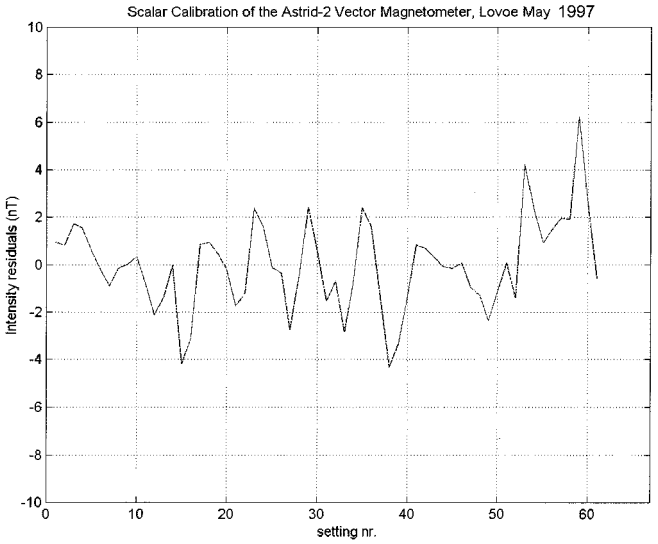

Fig. 6. Astrid-2 magnetometer pre-flight calibration at the Swedish magnetic observatory Lovoe on May 15–16, 1997. The 60 scalar field residuals shown have a standard deviation of 1.8 $\mathrm{nT_{rms}}$. The first 48 residuals corrected for a site gradient show 1.3 $\mathrm{nT_{rms}}$. The last 12 a value of 2.4 $\mathrm{nT_{rms}}$.

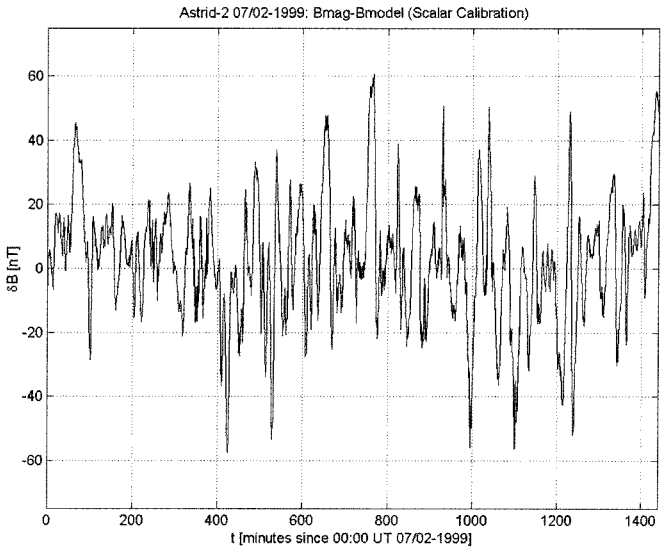

Fig. 7. Astrid-2 magnetometer in-flight calibration residuals by comparison with the IGRF95 model field extrapolated using the prospective secular variation. The standard deviation is about 18 $\mathrm{nT_{rms}}$.

between the actual slightly perturbed field at the satellite on February 7, 1999, and the predicted scalar value from the IGRF95.

The procedure of in-flight correcting the pre-flight calibration parameters is equivalent to the "analysis in payload coordinates" mentioned in the discussion section of [15]. For a well-distributed data set (the magnetic field covering all directions in the sensor coordinate system), it is generally accepted that adjusting the pre-flight calibration and at the same time constructing a model of the field is a convergent process yielding independent estimates of the calibration and modeling coefficients [16], [17]. Adjusting the magnetometer calibration leads to higher quality model coefficients, but does not influence the model apart from what follows from decreasing the overall data noise. An example of a short time series is given in Section IX.

VII. Main Field Model Derived From Scalar Data

In a current-free region, the magnetic field can be derived as the negative gradient of a scalar potential V, which is a function of the spatial coordinates (and also the time). Thus

$$\mathbf{B} = -\nabla V. \tag{3}$$

In the spherical geometry, as is suitable for geomagnetism, this scalar potential function is expanded using the spherical harmonics

$$V(r,\theta,\phi) = a\sum_{n=1}^{\infty}\sum_{m=0}^{n}\left[\left(\frac{a}{r}\right)^{n+1}(g_n^m\cos m\phi + h_n^m\sin m\phi) + \left(\frac{r}{a}\right)^{n}(q_n^m\cos m\phi + s_n^m\sin m\phi)\right]P_n^m(\cos\theta) \tag{4}$$

where a is the mean radius of the Earth ($a = 6371.2$ km), P_n^m are the associated Legendre polynomials of degree n and order m, g_n^m, h_n^m, q_n^m, s_n^m, are the Gauss coefficients, and (r, θ, ϕ) are the spherical coordinates: r is the distance, θ is the co-latitude and ϕ is the longitude. The coefficients g_n^m, h_n^m and q_n^m, s_n^m map the sources below and above the satellite altitude, respectively. The internal sources in the Earth's core are customarily modeled up to degree 13 because here the magnetic power spectrum has a knee. For n greater than 13, the wavelengths are of the order of or less than 3000 km, and their signature is associated with the crustal sources [18]. At the satellite altitude, there exists current systems and although some dynamic processes in the ionosphere have these spatial spectral characteristics, their signature is not static in general. Some of these current systems (specially in the auroral zones) cannot be modeled in a global sense and act like noise in the determination of the potential function. The magnetosphere is modeled by only three external coefficients reflecting the homogeneous field from the Equatorial ring current, and the time variation of the ring current is taken into account via the Dst index by [19]

$$\begin{aligned} q_1^0 &= +18.4 - 0.63\cdot Dst \\ q_1^1 &= -1.1 - 0.06\cdot Dst \\ s_1^0 &= -3.3 + 0.17\cdot Dst. \end{aligned} \tag{5}$$

The attitude of the magnetometer is not needed for estimating a main field model from scalar data. In this case, the intensity computed from the calibrated magnetometer M is used to determine the Gauss coefficients, thus

$$B = |\nabla V| = M. \tag{6}$$

A main field model derived from scalar data only, is known to be corrupted by the *Backus effect* [19]. There are tesseral terms of order $m = n$ that are not well resolved, as they are highly affected by noise and by unmodeled sources. This is due to the fact that an additional field perpendicular to the local field may exist, which can still produce nearly the same scalar value. When models derived from scalar data only are compared to models from vector data, believed to be the more correct ones, there may be large discrepancies around the dip Equator. These differences are most enhanced in the vertical component, and

they can be up to ± 2000 nT. Solutions to this problem can be devised when satellite vector data is not available, as is the case in the present work. The inclusion of vector data from geomagnetic observatories could be one possibility. Such data, however, are not evenly distributed over the globe being very sparse in the Southern hemisphere. Another solution is to constrain the model by some *a priori* knowledge of the position of the dip Equator. In other words, the positions, where the vertical component of the geomagnetic field is expected to decrease to a very small value, are used to force the model to attenuate the Backus discrepancy.

This has been implemented here in the following way: where ever the vertical component computed from the extrapolated IGRF95 model is within ± 2000 nT, then the predicted vertical component from the IGRF95 model is included alongside the observed scalar value. Here the assumption is that the relative time drift of the dip equator is smaller than the overall secular variation for the same period of time. This accounts for an increase of about 3% (55 extra points) of the total number of data points. A comparison of the resulting model with the extrapolated IGRF95 model is shown in Fig. 8. Since we are comparing two models, the high latitude data do not need to be discarded; furthermore, the errors of this comparison are larger in the Equatorial region. The overall rms value for the intensity (B), north ($-X$), east (Y), and radial ($-Z$) components are 18.0, 14.5, 7.6 and 18.6 $\mathrm{nT_{rms}}$, respectively. This means that the Backus effect has been heavily reduced by constraining the model only slightly, and the direction is resolved satisfactorily around the dip Equator. The discussion in [20], that "the error in the resulting model is simply constrained at the equator by our ability to update the location of this equator, and elsewhere by the quality of the scalar intensity data," applies equally well for the Astrid-2 scalar model.

The data (1766 scalar points) for the period chosen has produced a model whose scalar intensity is computed and plotted in Fig. 9. Because the data is equally spaced in time, a weighting factor has been introduced in order to simulate an even spatial distribution of the data over the surface of the Earth [19], [21]. The weighting factor depends only on the geographic co-latitude θ in the form $(\sin\theta)/5$, since the *a priori* overall error of the magnetic data due to unmodeled effects is estimated to be about 5 nT. A nonlinear least squares estimator is employed to obtain the coefficients of the main field model. The starting point is a tilted dipole (the IGRF95 model truncated to degree $n = 1$), and convergence is achieved in a few iterations.

The residuals show a characteristic pattern with the data fitting the model better in the Equatorial region where field-aligned currents are absent, while their presence in the Auroral zones is observed at high latitudes in Fig. 10. The misfit standard deviation for latitudes less than 50° is 4.54 $\mathrm{nT_{rms}}$, and the overall misfit including the polar caps is about 10 $\mathrm{nT_{rms}}$.

The rms scalar difference between the extrapolated IGRF95 model and the Astrid-2 model is significantly larger than the Astrid-2 model data scatter of 4.54 nT, indicating the significant change in the Earth's main magnetic field from what is predicted by a simple extrapolation of the IGRF. The resulting model is given in Table II, which matches the IGRF2000 [22] propagated

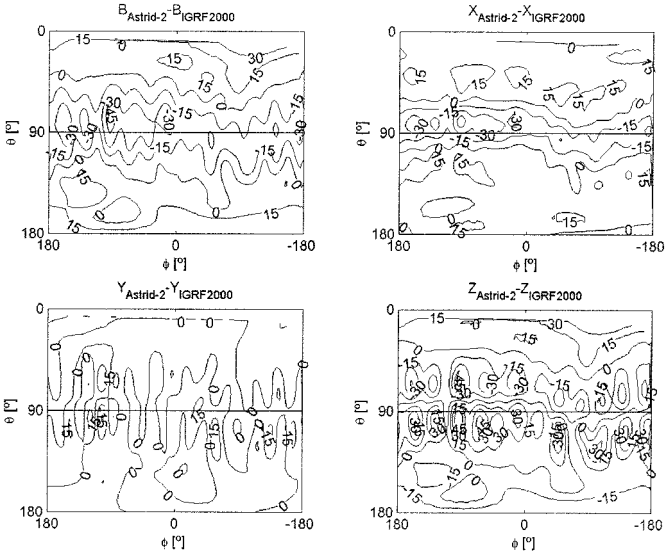

Fig. 8. Difference between the IGRF model and the Astrid-2 model derived from scalar data and constrained by the dip Equator position. The latitudinal stripes of the contour lines (in steps of 15 nT) are caused by the poor orbit distribution density, as shown in Fig. 5.

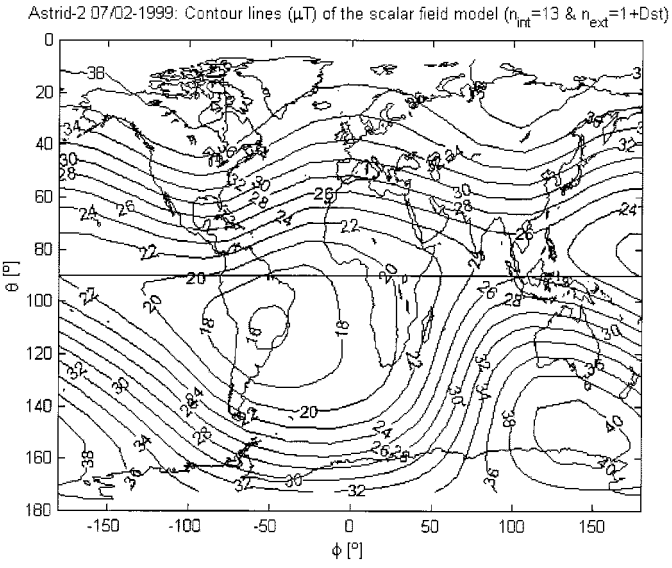

Fig. 9. Scalar field at satellite altitude computed from a magnetic main field model derived from February 7, 1999, scalar data measured by Astrid-2.

to the epoch of the period under examination here up to $n = 10$. However, it is worth noting than for degrees greater than 10 the coefficients are not resolved properly, since they are expected to decay as the degree increases. One reason for this behavior is that the altitude of Astrid-2 is probably too large for resolving these coefficients and that they may be contaminated by other sources such as currents crossing the satellite altitude and possibly by spatial aliasing of wavelengths shorter than about 1000 km. The covariance matrix (square matrix with dimension of the order of 200) is based on the data and weighting factors used. It shows that the ratio between the diagonal terms and the insignificant (in most cases) off-diagonal terms is up to orders of magnitude (see Table III), demonstrating that the orthogonality con-

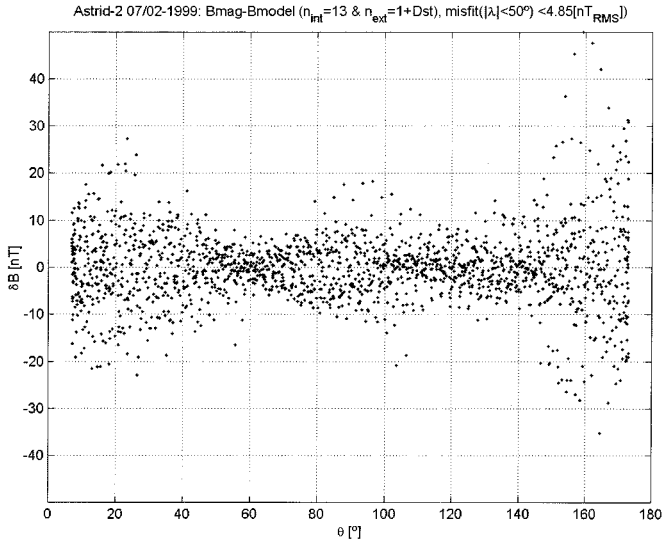

Fig. 10. Difference between the scalar magnetic field model and the scalar measurements of the Astrid-2 satellite for February 7, 1999, plotted against geographic co-latitude. The presence of the auroral regions is noticeable since the spherical harmonics model cannot account for the field-aligned currents.

dition of the spherical harmonic functions for the given dataset is partly fulfilled. Important is also the fact that the day was not extremely magnetically quiet and that time changes in the field will contribute to the data noise.

In order to investigate the significance of the higher degree terms, we have computed the low-latitude ($<50°$) scalar residuals of models of degrees 10, 11, and 12 to be 5.94, 5.70, and 5.17 nT, respectively. The higher than 10th degree terms thus only reduce the data spread slightly, and they are of minor significance in the model, as noted above.

The Danish Oersted satellite is dedicated to and designed for very accurate measurements of the vector components of the Earth's magnetic field. Comparison of the Astrid-2 data with those of Oersted indeed proves that the measurements of Astrid-2 are suitable for main field modeling. A combined Astrid-2/Oersted model of degree 13 for the internal static part (corrected with an internal secular variation of degree 8 from the IGRF2000) and degree 1 for the external contribution (in addition to a correction to the Dst dependency) has been derived by using Oersted data spanning a period in 1999 (OVH data from 17/3, 23/3 and 15/4; and both OVH and CSC data from 11–12/5, 17–18/5 and 12–22/5) and the Astrid-2 data set for February 7, 1999. The data used consist of: Oersted vector data from the fluxgate CSC magnetometer (1599 triple points), Oersted scalar data from the Overhauser OVH magnetometer (9431 points) and Astrid-2 scalar data (1766 points). Fig. 11 shows of the residuals of these data sets using a common model. Concentrating on the scalar residuals, Oersted gives a scalar misfit (latitude $<50°$) of 2.38 nT_{rms} whereas the Astrid-2 data has a standard deviation of only 4.48 nT_{rms} about the common model. The vector residual rms are: 5.48, 5.63 and 5.05 nT for the three components of the magnetic field (X, Y, Z), respectively. Oersted was designed to provide vector components with this accuracy, whereas the main purpose of the Astrid-2 magnetometer was to provide high time-resolution data suited for auroral studies. This comparison supports the claim of very high stability and mapping quality of the Astrid-2 science magnetometer, and the absence of a bias in the Astrid-2 data compared to the Oersted data constitutes an independent test of the success of the in-flight adjustment of the Astrid-2 pre-flight calibration Therefore, the Astrid-2 data set is self-consistent and consistent with the Oersted data.

TABLE II
MAIN FIELD MODEL COEFFICIENTS

n	m	g_{nm} (nT)	h_{nm} (nT)	n	m	g_{nm} (nT)	h_{nm} (nT)
1	0	-29626.90	0	10	0	-0.89	0
1	1	-1741.30	5201.04	10	1	-5.24	3.62
2	0	-2254.10	0	10	2	2.72	-0.41
2	1	3068.72	-2460.88	10	3	-4.00	3.70
2	2	1671.61	-450.87	10	4	-0.47	4.50
3	0	1322.81	0	10	5	4.25	-5.39
3	1	-2285.70	-222.54	10	6	1.17	-1.76
3	2	1253.77	296.23	10	7	2.71	-2.27
3	3	722.81	-481.47	10	8	3.66	2.27
4	0	930.20	0	10	9	-1.68	-1.05
4	1	786.86	269.25	10	10	-0.15	-7.16
4	2	260.21	-232.13	11	0	1.84	0
4	3	-407.75	114.95	11	1	-0.99	1.41
4	4	113.59	-301.19	11	2	-3.03	0.96
5	0	-209.75	0	11	3	1.29	-0.43
5	1	350.66	37.56	11	4	0.09	-2.80
5	2	223.27	170.16	11	5	-1.34	-0.09
5	3	-127.84	-134.54	11	6	0.81	-1.13
5	4	-168.17	-44.20	11	7	0.35	-2.67
5	5	-13.76	106.82	11	8	1.69	-1.23
6	0	75.27	0	11	9	-1.54	3.13
6	1	67.74	-15.13	11	10	-1.02	-2.86
6	2	73.08	64.79	11	11	3.50	-1.09
6	3	-162.74	65.14	12	0	-1.40	0
6	4	-3.95	-60.12	12	1	1.06	2.20
6	5	16.40	3.42	12	2	1.84	0.86
6	6	-89.99	41.71	12	3	0.10	1.41
7	0	75.27	0	12	4	-1.13	-1.29
7	1	-72.22	-61.86	12	5	1.99	1.75
7	2	-0.21	-25.15	12	6	-1.04	0.54
7	3	31.95	6.28	12	7	-0.46	-0.62
7	4	9.27	24.01	12	8	-2.34	0.44
7	5	8.72	16.72	12	9	-2.63	0.79
7	6	6.87	-23.57	12	10	-5.73	-0.70
7	7	-1.74	-5.88	12	11	-0.33	-6.18
8	0	24.12	0	12	12	-2.86	-4.76
8	1	7.37	13.63	13	0	-0.52	0
8	2	-6.84	-21.54	13	1	-0.05	-1.19
8	3	-9.37	7.41	13	2	-0.95	-0.93
8	4	-16.72	-21.39	13	3	-0.08	1.77
8	5	8.41	15.64	13	4	-0.96	-0.70
8	6	6.05	8.56	13	5	0.48	-1.87
8	7	-5.41	-14.15	13	6	-0.70	-0.21
8	8	-7.31	-1.51	13	7	1.73	1.79
9	0	5.02	0	13	8	-0.30	-0.48
9	1	9.07	-21.28	13	9	1.37	1.27
9	2	1.24	12.33	13	10	-1.08	2.16
9	3	-7.66	12.74	13	11	5.61	-0.95
9	4	5.55	-5.85	13	12	-2.36	10.80
9	5	-8.45	-9.44	13	13	5.74	-1.71
9	6	-0.98	9.55				
9	7	8.13	2.87				
9	8	-0.71	-7.94				
9	9	-7.71	4.18				

Coefficients of the main field model up to degree 13 and derived from the Astrid-2 February 7, 1999 scalar data.

TABLE III
COVARIANCE MATRIX COEFFICIENTS

	(μT)	C_{ii}	$C_{(i+1)i}$	$C_{(i+2)i}$		(μT)	C_{ii}	$C_{(i+1)i}$	$C_{(i+2)i}$
g_{10}	-29.62	184.16	5.72	-27.02	g_{42}	0.26	96.54	0.46	4.41
g_{11}	-1.74	30.34	-0.42	-6.35	h_{42}	-0.23	92.94	3.74	3.16
h_{11}	5.20	37.56	2.93	0.25	g_{43}	-0.40	82.76	-1.66	-0.62
g_{20}	-2.25	118.51	7.62	6.95	h_{43}	0.11	83.03	17.17	0.54
g_{21}	3.07	135.16	-0.24	-2.31	g_{44}	0.11	16.47	0.37	-0.58
h_{21}	-2.46	142.56	23.69	5.91	h_{44}	-0.30	17.09	0.42	1.46
g_{22}	1.67	27.87	1.75	9.69	g_{50}	-0.21	99.04	0.69	-1.28
h_{22}	-0.45	23.02	-0.90	0.80	g_{51}	0.35	96.94	-0.06	2.89
g_{30}	1.32	131.95	1.14	-7.49	h_{51}	0.04	97.12	2.32	1.57
g_{31}	-2.29	108.97	-0.76	5.41	g_{52}	0.22	90.86	0.16	2.79
h_{31}	-0.22	112.72	2.03	4.60	h_{52}	0.17	87.86	5.18	1.51
g_{32}	1.25	108.94	1.35	1.31	g_{53}	-0.13	77.74	-1.08	2.12
h_{32}	0.30	105.49	18.77	-0.13	h_{53}	-0.13	78.40	5.48	3.29
g_{33}	0.72	20.66	-1.03	-1.04	g_{54}	-0.17	63.30	1.21	0.24
h_{33}	-0.48	20.36	2.17	-1.07	h_{54}	-0.04	64.57	14.72	-0.94
g_{40}	0.93	112.81	2.29	0.86	g_{55}	-0.01	14.00	-0.22	-0.74
g_{41}	0.78	109.37	0.00	1.86	h_{55}	0.11	13.46	-0.27	0.25
h_{41}	0.27	110.39	6.49	2.44					

Diagonal (C_{ii}), 1st Off-Diagonal ($C_{(i+1)i}$) and 2nd Off-Diagonal ($C_{(i+2)i}$) elements of the Covariance Matrix (only up to n=5) for the inversion using the data set to obtain the model of table II

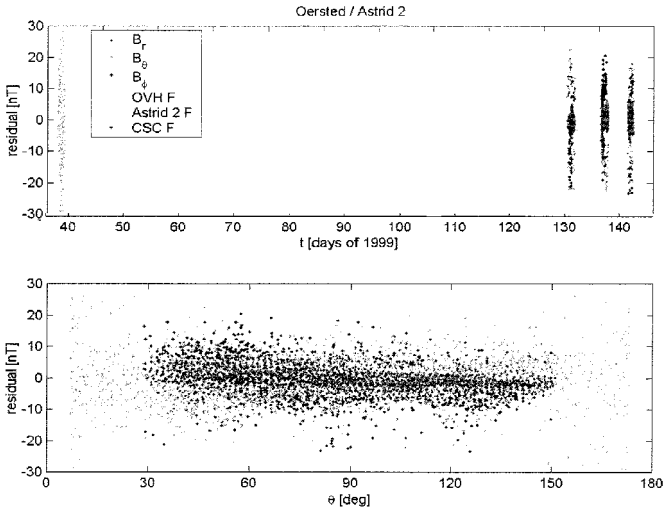

Fig. 11. Astrid-2 scalar data (as function of co-latitude θ) for February 7, 1999 (cyan color) compared to the data of the dedicated geomagnetic satellite Oersted. The spread of the scalar measurements are 2.38 nT_{rms} and 4.48 nT_{rms} for Oersted and Astrid-2, respectively. (Courtesy of N. Olsen, Danish Space Research Institute.)

VIII. ATTITUDE RECOVERY AND VECTOR FIELD MODELING

The attitude of the magnetometer has to be known to a certain accuracy for two main reasons. Firstly, if vector data is going to be used for main field vector modeling, geomagnetic research or external field sources investigation, it is important to very accurately determine the absolute orientation of the vector magnetometer coordinate system. Secondly, if it is possible to establish the orientation of the magnetometer in a reference system, Earth or Sun related, then it is also possible to determine the attitude of the spacecraft.

It was previously proposed [23] that the process of modeling the Earth's main magnetic field and at the same time to model the dynamics of the spacecraft, i.e., the magnetometer coordinate system absolute orientation, would yield independent estimates of the magnetic field model and of the satellite dynamics matching the on-board measured magnetic field components. The problem has to consider the vast class of spacecraft dynamics modes, force-free or under attitude and orbit control actions. Even so-called "force-free" dynamics will have to take into account a number of dynamics perturbing residual forces and effects, if arcsec accuracy in the attitude is desired. The spin axis is fairly fixed in an inertial frame but there are some modulations that have to be corrected for. The simplest types of motions will have to be considered first in order to investigate the feasibility of simultaneous dynamics and magnetic field modeling.

Astrid-2 is a spinning satellite with the spin axis normal to the solar panels and a spin frequency of the order of 9 rpm. The stable flat spin of the satellite about the body axis of maximum moment of inertia constitutes a very basic and simple motion and ensures an almost constant attitude of the spin axis in inertial space, and therefore the accomplished stability of the satellite is conceptually simple to model. In the following, the observed dynamic stability of the Astrid-2 satellite is demonstrated based exclusively on magnetic data, and the prospects for modeling the dynamics to the arcsec level are discussed.

Let $\mathbf{M}$ be the calibrated magnetometer measurements in the magnetometer reference system and $\mathbf{M}^{SR}$ the magnetic field in a coordinate system having one of the axes parallel to the spin axis, i.e., the spin motion is not seen in that component of the magnetic field (see Fig. 12), whereas the other two components see the spin with a relative phase of 90°. $\mathbf{M}^{S}$ is the corresponding magnetic field in the despun inertial coordinate system (not shown). The measurements in the magnetometer reference system, and in the spin-axis-aligned inertial system are related by three rotation matrixes R_1, R_2, and R_3

$$\mathbf{M}^{S} = R_1(\Phi)R_2(\beta)R_3(\alpha)\mathbf{M}. \tag{7}$$

The alignment angles α and β are very small under the assumption that the x axis of the magnetometer is almost aligned to the spin axis (the mounting orientation of the sensor has been designed in this way). The spin phase is introduced in Φ, which is related to the spin frequency ω by

$$\Phi = \omega t + \Phi_0 \tag{8}$$

where Φ_0 is a reference phase angle, and t is the time.

The observed alignment angles are plotted in Fig. 13 as functions of time for several orbits. A pair of angles (α and β) are estimated by using a few spin periods of magnetometer calibrated data, and this is repeated consecutively. The quality of the solution for the angles depends upon the variation of the magnetic field, and that is the reason why it is not possible to determine a solution with enough accuracy in the polar caps (see the gaps in Fig. 13). As assumed above, these angles are small with mean values of less than one degree. Their long term variation with time is within 60 arcsec peak-to-peak or of the order of one hundredth of a degree over several orbits.

The magnetometer thus "sees" the Earth's magnetic field vector spinning about a definite axis in the magnetometer system. Above, this axis is identified with the satellite spin axis, because the magnetometer sensor is fixed to the satellite. Assuming for a moment that the spin axis is constant in inertial

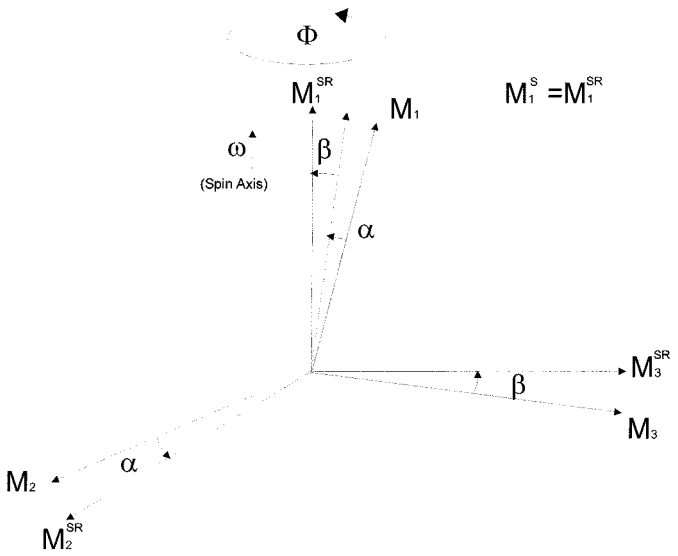

Fig. 12. Astrid-2 magnetometer system $\mathbf{M}$ and the spin-axis-related satellite reference system $\mathbf{M}^{SR}$ that spins about the M_1^{SR} component. The corresponding despun system is represented by $\mathbf{M}^S$ (only first component shown).

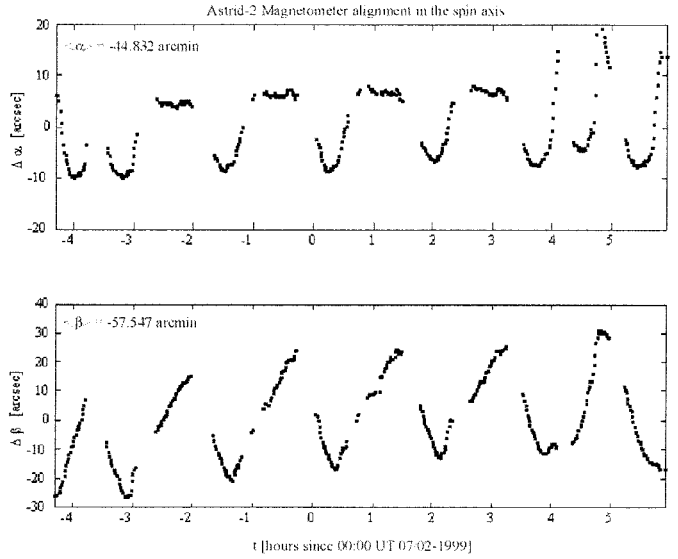

Fig. 13. The time evolution of the alignment angles α and β with respect to the mean value ($\langle\alpha\rangle = -44.832$ arcmin and $\langle\beta\rangle = -57.547$ arcmin) for six whole orbits. These angles are used to transform the data into a spin axis aligned reference system. Their peak-to-peak variation is less than 20 and 60 arcsec, repectively.

space, then some orbit-related variations in the angles α and β are to be expected, because the Earth's main field vector slowly changes direction in inertial space over the orbit. This effect is, of course, included in the 60-arcsec overall variation, and it can be modeled and compensated for.

Another cause of orbit-related changes in α and β follows from the fact that the hinged boom placing the magnetometer sensor away from the spacecraft body is supported by a stay holding it in position (see Fig. 1), and this stay will contract and expand with the changing temperature along the orbit, thereby slightly rotating the magnetic sensor axis M_1 about the boom hinge relative to the satellite spin axis in the 1–3-plane. This would explain the temporal periodic variation of the β angle. Still, this effect is also contained in the observed 60 arcsec variation.

Any variation of the mass distribution of the satellite, including the flexible light-weight $\mathbf{E}$-field probe wire booms and the science magnetometer sensor, will violate the rigid body assumption of a constant spin vector in inertial space, and such changes will also be reflected in the variation of the α angle as well as of the β angle.

The fact that all these effects, and other perturbations not considered here, give no more than 60 arcsec changes over several orbits in the apparent direction of the spin axis, holds great promises for further work aimed at modeling and compensating for the observed variations. A factor-of-5 improvement in the knowledge of the apparent spin axis orientation to ± 6 arcsec corresponds to less than ± 2 nT in the 40 000-nT field. Further work on modeling the satellite dynamics will investigate the feasibility of this.

In order to despin the data, the spin frequency ω also has to be known to a very high accuracy. In the ideal case, the spin frequency would be constant. But it has been found that this is not quite the case, as the frequency varies periodically and related to the orbital phase. Once again, any change of the moments of inertia of the spacecraft due to mass distribution changes would influence the spin frequency. Also, the slow change (compared to the spin period) of the inertial direction of the Earth's magnetic field vector along the orbit will influence the spin rate, and this has not yet been taken into account in this preliminary investigation. This means that it is not a straightforward task to despin the magnetic data in the spin plane to the required accuracy, and any error introduced into this parameter would propagate directly to the orientation accuracy of the vector components. An example of de-spun data is given in the next section.

The accuracy needed for obtaining the vector components should be better than ± 6 arcsec as mentioned above. Presently, efforts are made to use all of the vector magnetic information from the Astrid-2 science magnetometer. This will be the subject of a forthcoming publication. The idea is that if the magnetic data is presented in an inertial reference frame (that of the spin axis) in which one component of the data is aligned to the spin axis and the other two components are accurately despun, it is believed possible to solve simultaneously for the attitude of the magnetometer and the Gauss coefficients of the main field model spherical harmonic expansion. Thus

$$\mathbf{B} = -\nabla V = R_{\mathrm{ECEF}}(t)R_3(\gamma_1)R_2(\gamma_2)R_3(\gamma_3)\mathbf{M}^S \qquad (9)$$

where the angles γ_1, γ_2, and γ_3 are an alternative way of representing the spin axis direction and the offset phase Φ_0. These angles may be time-dependent, and the time changes will have to be modeled. R_{ECEF} is the transformation that brings the spin aligned reference system into an Earth-Centered–Earth-Fixed system and it depends on time t.

IX. Observation of Auroral Zone Field-Aligned Currents

Another feature worth mentioning is the crossing of the auroral zones by Astrid-2, where field-aligned currents are present. This is shown in Fig. 14 for a short period during February 7,

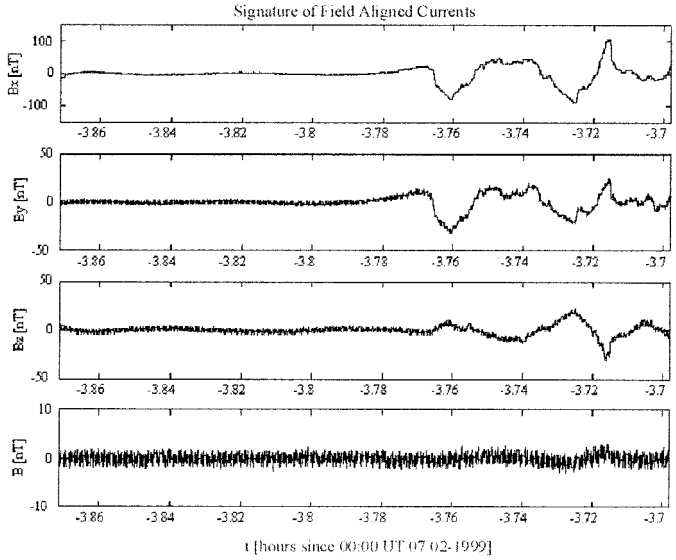

Fig. 14. Astrid-2 magnetometer data detecting the crossing of current sheets in the auroral zone (in the spin-axis-aligned inertial system). The signature is present in the vector components while the total intensity remains virtually constant (1 $\mathrm{nT_{rms}}$). The equivalent current density is about 0.8 $\mu\mathrm{A/m^2}$.

1999. The magnetic data are presented in the despun spin-axis-aligned inertial system and detect a feature that resembles the crossing of a sheet of current, since only the direction of the field is changed, while the scalar magnitude is practically invariant to below the 1-$\mathrm{nT_{rms}}$ level. The current density is determined to be about 0.8 $\mu\mathrm{A/m^2}$.

X. Discussion and Conclusion

The magnetic data of the Astrid-2 science magnetometer are proven to be of a very high quality for geomagnetic research. After in-flight adjustment of the pre-flight calibration, the standard deviation of the scalar data about the Astrid-2 Earth's field model was less than 5 nT, and an independent comparison with the Oersted data showed similarly less than 5 nT spread about the model and no bias. The combined Astrid-2/Oersted model is mainly determined by Oersted, as the Astrid data only constitute a very small fraction of the total data set.

The satellite did not carry any device for position determination, and the orbit was reconstructed by using the NORAD subroutine and two-line-elements. It is believed that the position accuracy is better than 1 km in all three components since a 1-km uncertainty in all directions would give a misfit of 10 nT in the geomagnetic model since the data standard deviation about a fitted model was less than 5 nT. The positional accuracy, though, is not better than 0.1 km. There is not a general procedure to check the positioning error derived from TLEs. However, it is possible to check the consistency of the TLEs by comparing the computed positions at the same epoch derived from consecutive TLEs. This has been done for the period of February 7, 1999, confirming that the consistency is of the order of 100 m.

The timing accuracy is stated by the project to be in all cases better than 0.1 s. This is confirmed by our results, because 0.1 s timing error translates to about 700 m along track giving about a 1.5-nT error in the scalar field. The error in this direction in the plane of the orbit is slightly larger than the altitude error due to geometry considerations (the altitude is precisely related to the period and the plane is inertial).

A high-precision attitude of the magnetometer is needed for accomplishing a vector model. This has been suggested by relating the reference system to the spin axis and determining the initial spinning phase and the spin frequency. The simplest dynamic situation for this is during periods when no attitude or orbital maneuvers of the spacecraft take place. The rotation axis of the magnetic field was determined in the magnetometer coordinate system. This rotation axis stayed constant in the magnetic sensor within 60 arcsec peak-to-peak over several orbits, with the perturbations being orbital phase dependent. This opens for the possibility of simultaneously modeling the satellite dynamics and the Earth's magnetic field.

The successful use of the scalar data to achieve a main field model with a misfit of less than 5 nT away from the auroral zones, brings extremely good prospects for the Astrid-2 data. The altitude of 1000 km, the polar proximity of the orbit, the drift rate of the orbital plane covering all local times, and the combination with other geopotential fields missions like Oersted, CHAMP, and SAC-C enhances the potential of the satellite for space physics and geomagnetic research.

References

[1] R. A. Langel, G. Ousley, J. Berbert, and M. Settle, "The MAGSAT mission," *Geophys. Res. Lett.*, vol. 9, pp. 243–245, 1982.

[2] G. T. Marklund, L. Blomberg, L. Bylander, and P.-A. Lindqvist, "Astrid-2: A low-budget microsatellite mission for auroral research," in *Proc. ESA Symp. European Rocket and Balloon Programmes and Related Research*, Borgholm (Oeland), Sweden, May 26–29, 1997, ESA SP-397, pp. 387–394.

[3] T. Bak, "Spacecraft attitude determination—A magnetometer approach," Ph.D. dissertation, Dept. of Control Engineering, Aalborg Univ., Aalborg Oe, Denmark, 1999.

[4] J. M. G. Merayo, "Magnetic gradiometry," Ph.D. dissertation, Tech. Univ. Denmark, Lyngby, 1999.

[5] J. M. G. Merayo, P. Brauer, F. Primdahl, and J. R. Petersen, "Absolute magnetic calibration and alignment of vector magnetometers in the Earth's magnetic field," in *Worshop on Calibration of Space-Borne Magnetometers in Ground and In-Flight Space Magnetometer Calibration Techniques*, Braunschweig, Germany, Mar. 1999, ESA SP-490.

[6] O. V. Nielsen, J. R. Petersen, F. Primdahl, P. Brauer, B. Hernando, A. Fernández, J. M. G. Merayo, and P. Ripka, "Development, construction and analysis of the Oersted fluxgate magnetometer," *Meas. Sci. Technol.*, vol. 6, pp. 1099–1115, 1995.

[7] P. Brauer, T. Risbo, J. M. G. Merayo, and O. V. Nielsen, "Fluxgate sensor for the vector magnetometer onboard the Astrid-2 satellite," *Sens. Actuators A*, vol. 81, pp. 184–188, 2000.

[8] E. B. Pedersen, F. Primdahl, J. R. Petersen, J. M. G. Merayo, P. Brauer, and O. V. Nielsen, "Digital fluxgate magnetometer for the Astrid-2 satellite," *Meas. Sci. Technol.*, vol. 10, pp. 124–129, 1999.

[9] J. M. G. Merayo, P. Brauer, T. Risbo, E. B. Pedersen, J. R. Petersen, and F. Primdahl, "Astrid-2 EMMA magnetic calibration," Tech. Univ. Denmark, Lyngby, Tech. Rep. Astrid-2 satellite (1–25), July 1998.

[10] J. M. G. Merayo, P. Brauer, F. Primdahl, J. R. Petersen, and O. V. Nielsen, "Scalar calibration of vector magnetometers," *Meas. Sci. Technol.*, vol. 11, pp. 120–132, 2000.

[11] J. M. G. Merayo, F. Primdahl, P. Brauer, T. Risbo, N. Olsen, and T. Sabaka, "The orthogonalization of magnetic systems," *Sens. Actuators A, Phys.*, vol. 89, pp. 185–196, 2001.

[12] [Online]. Available: ftp://ftp.gfz-potsdam.de/pub/home/obs/kp-ap/tab/kp9902.ps

[13] [Online]. Available: http://swdcdb.kugi.kyoto-u.ac.jp/dstdir/dst1/f/dstfinal199 902.html

[14] [Online]. Available: http://celestrak.com/
[15] J. E. P. Connerney, "The magnetic field of jupiter: A generalized inverse approach," *J. Geophys. Res.*, vol. A-9, pp. 7679–7693, 1981.
[16] T. J. Sabaka, J. A. Conrad, J. M. G. Merayo, and R. A. Langel, "Analysis of defence meteorological satellite program 12 and 13 satellite magnetometer measurements," GSFC-NASA, Tech. Rep. HSTX/G&G-9702, (1–69), Feb. 1997.
[17] R. A. Langel, J. A. Conrad, T. J. Sabaka, and R. T. Baldwin, "Adjustment of UARS, POGS, and DE-1 satellite magnetic field data for modeling of the Earth's main field," *J. Geomag. Geoelect.*, vol. 49, pp. 393–415, 1997.
[18] M. G. McLeod and P. J. Coleman, Jr., "Spatial power spectra of the crustal geomagnetic field and core geomagnetic field," *Phys. Earth Planetary Interiors*, vol. 23-2, pp. 5–19, 1980.
[19] G. E. Backus, "Non-uniqueness of the external geomagnetic field determined by surface intensity measurements," *J. Geophys Res.*, vol. 75, pp. 6337–6341, 1970.
[20] P. Ultré-Gérard, M. Hamoudi, and G. Hulot, "Reducing the backus effect given some knowledge of the dip equator," *Geophys. Res. Lett.*, vol. 25, pp. 3201–3204, 1998.
[21] R. A. Langel, "The main geomagnetc field," in *Geomagnetism*, J. A. Jacobs, Ed. New York: Academic, 1987, vol. 2, pp. 249–512.
[22] N. Olsen, R. Holme, G. Hulot, T. Sabaka, T. Neubert, L. Toeffner-Clausen, F. Primdahl, J. Joergensen, J.-M. Lèger, D. Barraclough, J. Bloxham, J. Cain, C. Constable, V. Golovkov, A. Jackson, P. Kotzé, B. Langlais, S. Macmillan, M. Mandea, J. Merayo, L. Newitt, M. Purucker, T. Risbo, M. Stampe, A. Thomson, and C. Voorhies, "Oersted initial field model," *Geophys. Res. Lett.*, vol. 27-22, pp. 3607–3610, 2000.
[23] J. C. Cain, Z. Wang, and D. R. Schmitz, "A simple monitor of the geomagnetic field," *EOS*, vol. 66, p. 861, 1985.

Jose M. G. Merayo, photograph and biography not available at the time of publication.

Peter Brauer, photograph and biography not available at the time of publication.

Fritz Primdahl, photograph and biography not available at the time of publication.

Peter S. Joergensen, photograph and biography not available at the time of publication.

Torben Risbo, photograph and biography not available at the time of publication.

Joe Cain, photograph and biography not available at the time of publication.